AIAA SciTech Forum
8-12 January 2024, Orlando, FL
AIAA SCITECH 2024 Forum

10.2514/6.2024-1727

Flapped CoFlow Jet Airfoil for High Lift Cruise at Low Reynolds Number in Martian Atmosphere

Jaehyoung Jeon * Yan Ren † Gecheng Zha ‡
Dept. of Mechanical and Aerospace Engineering
University of Miami, Coral Gables, Florida 33124
E-mail: gzha@miami.edu

Abstract

The development of fixed wing aircraft for Mars exploration is desirable, but needs to overcome the challenge of low Reynolds number due to thin Martian atmosphere. Flapped CoFlow jet(FCFJ) airfoil has the potential to achieve an ultra-high cruise lift coefficient with acceptable corrected aerodynamic efficiency of $C_L/(C_D + Pc)$. This study investigates whether FCFJ airfoils and regular CFJ airfoils can have high aerodynamic performance at cruise condition at three cruise Mach number 0.17, 0.26 and 0.4, which have the corresponding Reynolds number of 5.43×10^4, 1.42×10^5 and 2.18×10^5, respectively. The regular CFJ airfoil applies the injection very close to the leading edge at about 2-4% chord location. The FCFJ airfoil has a long flap with the CFJ applied inside the flap as part of the airfoil. The research is based on validated CFD simulation using a 2D RANS solver with Spalart-Allmaras(SA) turbulence model, a third-order WENO scheme for the inviscid fluxes, and second-order central differencing for the viscous terms. At a Mach number of 0.26, numerical simulations show that the FCFJ airfoil can obtain a cruise lift coefficient of 3.74, a lift-to-drag ratio (C_L/C_D) of 172.54, and a corrected aerodynamic efficiency of 20.5. At the Mach number of 0.17, the FCFJ flow is mostly incompressible and the aerodynamic efficiency slightly lower than that at Mach number of 0.26. At freestream Mach number of 0.4, the flow reaches supersonic and makes it very difficult to attach. The study indicates that the FCFJ airfoil is promising for a fixed wing aircraft to fly on Mars.

Nomenclature

CFJ	CoFlow jet
$FCFJ$	Flapped CoFlow jet
$AoA(\alpha)$	Angle of attack
β	Deflection angle
LE	Leading Edge
TE	Trailing Edge

* Ph.D. Student
† Postdoc Researcher, Ph.D., AIAA member
‡ Professor, ASME Fellow, AIAA associate Fellow

s	Wing Span length
c	Profile chord
U	Flow velocity
q	Dynamic pressure $0.5\,\rho\,U^2$
p	Static pressure
ρ	Air density
P	Pumping power
C_L	Lift coefficient $L/(q_\infty\,S)$
C_D	Drag coefficient $D/(q_\infty\,S)$
C_μ	Jet momentum coef. $\dot{m}_j\,U_j/(q_\infty\,S)$
Pc	Power coefficient $L/(q_\infty\,S\,V_\infty)$
$(C_L/C_D)_c$	CFJ airfoil corrected efficiency $C_L/(C_D$+Pc)
R_e	Reynolds number
M	Mach number
c_p	Constant pressure specific heat
γ	Air specific heats ratio
S	Planform area of the wing
T_t	Total temperature
P_t	Total pressure
H_t	Total specific enthalpy
$\dot{m}$	Mass flow across the pump
$_\infty$	Subscript, stands for free stream
$_j$	Subscript, stands for jet

1 Introduction

Recently, interest and research in Mars exploration and colonization have grown significantly. Technologies, such as launch vehicles like SpaceX's Starship, suggest that the day when humans can journey to Mars is not too far in the future. Mars, with its vast and diverse landscape, presents numerous challenges and opportunities for human exploration and settlement. The development of high-performance, high-efficiency aircraft designed specifically for the Martian environment is essential to meeting these challenges and achieving our goals. By providing enhanced mobility and accessibility for exploration of the vast terrain, such aircraft can play a critical role in accelerating science missions to discover the geology history of Mars, finding evidence of past life, resource discovery, and identifying suitable locations for base camps.

One of the key challenges in developing these aircraft is to efficiently generate sufficient lift in the low Reynolds number due to low-density Martian atmosphere. Addressing these issues will not only deepen our understanding of the Martian environment, but also pave the way for sustainable colonization and the future of human space exploration. Due to Mars' significantly lower atmospheric density compared to Earth, innovative technologies are required to develop aircraft capable of operating in such challenging conditions. Earth-based aircraft rely on the interaction between air and their wings to generate lift, which allows them to remain airborne. However, Mars' thin atmosphere, which is about 100 times less dense than Earth's, poses a considerable challenge in generating the required lift to keep an aircraft aloft in the Martian environment. The distinct atmospheric characteristics on Mars demand a different

approach to aerodynamic design to ensure optimal performance. Aircraft designed for Mars may need larger wingspans, lower wing loading, and unique control surfaces tailored to the planet's atmospheric conditions[1].

Witold et al.[2] explained that "At Reynolds numbers below approximately 500,000, conventional airfoils lose aerodynamic efficiency. This is because at lower Reynolds numbers, viscous forces become stronger relative to inertial forces, leading to a delay in the transition from laminar to turbulent flow. Additionally, the increased boundary layer thickness at lower Reynolds numbers can reduce lift coefficient, although the impact on lift is generally less significant than the increase in drag coefficient." For these reasons, conventional airfoils at low Reynolds numbers have unfavorable aerodynamic properties.

The purpose of this paper is to study a new airfoil configuration for Martian flight at low Reynolds number, flapped coflow jet (FCFJ) airfoil, which demonstrates high cruise lift coefficient at high Reynolds number [3, 4]. This study is to show that the same concept is also promising for low Reynolds number environment on Mars.

1.1 CoFlow Jet Airfoil

Active flow control (AFC) with energy added to the flow has attracted a lot of interest to increase C_{Lmax} by suppressing flow separation to increase airfoil circulation. However, using AFC for cruise is challenging because the benefit gained may not be able to offset the AFC energy consumed for the overall aircraft system to achieve a net efficiency gain. One promising AFC that has the potential to increase cruise efficiency is the CoFlow Jet (CFJ) flow control airfoil[5, 6, 7, 8, 9, 10, 11, 12, 13, 14, 15, 16, 17, 18, 19, 20]. For a regular CFJ airfoil, as shown in Fig. 1, a small amount of mass flow is drawn into the suction duct, pressurized and powered by a pump, and then injected near the LE tangentially to the main flow. The CFJ AFC is thus a zero-net-mass-flux (ZNMF) flow control, which has only energy exchange with the controlled flow system with no mass exchange. In comparison with the 2D baseline airfoil, Wang and Zha[21] show that the 2D CFJ airfoil can achieve a significantly higher cruise lift coefficient and aerodynamic efficiency, defined as

$$(\frac{C_L}{C_D})_c = \frac{C_L}{C_D + P_c} \tag{1}$$

where Pc is the CFJ required power coefficient. However, for 3D wings with finite aspect ratios, the CFJ wings can still maintain high cruise C_L, but the aerodynamic efficiency is decreased to the level of its baseline counterparts [22]. To reflect the transportation productivity of aircraft represented by the range multiplied by the gross weight, a cruise productivity efficiency is introduced as [16]:

$$(\frac{C_L^2}{C_D})_c = \frac{C_L^2}{(C_D + Pc)} \tag{2}$$

CFJ wing can have substantially higher cruise C_L and thus greater productivity efficiency as well. Taking advantage of the CFJ wing high cruise lift coefficient and thus high suction effect on wing upper surface, Ren and Zha [23] design a tandem wing aircraft configuration that the front wing tip vortex is captured by the rear wing to enhance the overall system efficiency. However, for cruise condition, the regular CFJ configuration as shown in Fig. 1 appears to have rapid energy consumption increase when C_L is greater than 1.6[16, 24]. Even though the aerodynamic drag coefficient C_D can remain small and

the pure aerodynamic lift to drag ratio C_L/C_D can be still very high, the corrected aerodynamic efficiency defined in Eq. (1) can decrease quickly with the increasing C_L.

The flapped CFJ has been found to achieve very high C_L while maintaining reasonable $(C_L/C_D)_c$ [3, 4]. This technology can compensate the lift force due to low density at altitudes of about 30,000 meters on Earth or Mars, and will be helpful in performing various missions. In this study, we numerically analyze the characteristics of the flapped CFJ under low Reynolds number conditions caused by very thin density.

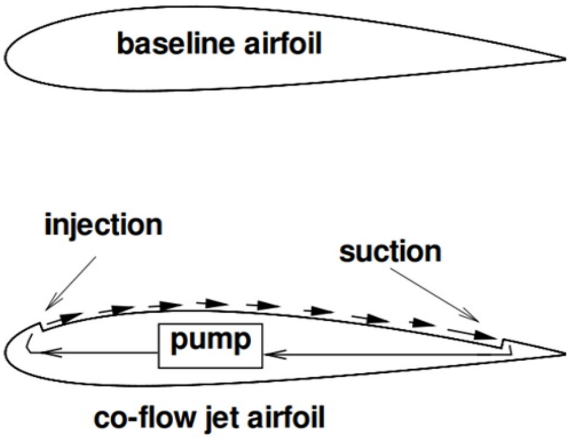

Figure 1: Sketch of CoFlow Jet airfoil

1.2 Flapped CoFlow Jet Airfoil

The concept of flapped coflow jet airfoil is adopted from the CFJ airfoil with deflected slipstream for VTOL aircraft [25]. It is also guided by the CoFlow jet flow separation mechanism study of Xu and Zha [26].

The CFJ is applied inside a long flap that is a part of the flapped CFJ airfoil, as shown in Fig.2 [3], which has the injection located at the shoulder of the flap. The regular CFJ airfoil applies the injection very close to the leading edge at a point of around 2-4% chord location. By deflecting the flap rather than rotating the front part of the airfoil, the FCFJ airfoil has the advantage of allowing the airfoil to increase the angle of attack and lift coefficient without tilting the wings or the propeller. Previous studies demonstrates high cruise lift coefficient at high Reynolds number for FCFJ airfoil [3, 4]. This study is to show that the same concept is also promising for low Reynolds number environment on Mars.

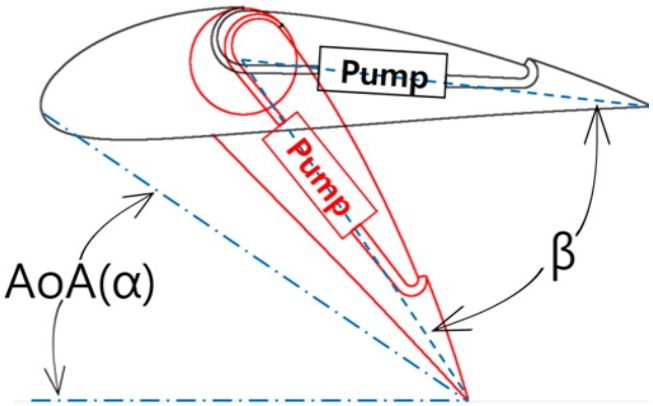

Figure 2: Sketch of flapped CFJ airfoil with the CoFlow jet applied on the flap

2 Methodology

2.1 Lift and Drag Calculation

The momentum and pressure at the injection and suction slots produce a reactionary force, which is automatically measured by the force balance in wind tunnel testing. However, for CFD simulation, the full reactionary force needs to be included. Using control volume analysis, the reactionary force can be calculated using the flow parameters at the injection and suction slot opening surfaces. Zha et al. [6] give the following formulations to calculate the lift and drag due to the jet reactionary force for a CFJ airfoil. By considering the effects of injection and suction jets on the CFJ airfoil, the expressions for these reactionary forces are given as :

$$F_{x_{cfj}} = (\dot{m}_j V_{j1} + p_{j1} A_{j1}) * cos(\theta_1 - \alpha) - (\dot{m}_j V_{j2} + p_{j2} A_{j2}) * cos(\theta_2 + \alpha) \tag{3}$$

$$F_{y_{cfj}} = (\dot{m}_{j1} V_{j1} + p_{j1} A_{j1}) * sin(\theta_1 - \alpha) + (\dot{m}_{j2} V_{j2} + p_{j2} A_{j2}) * sin(\theta_2 + \alpha) \tag{4}$$

where the subscripts 1 and 2 stand for the injection and suction respectively, and θ_1 and θ_2 are the angles between the injection and suction slot's surface and a line normal to the airfoil chord. α is the angle of attack.

The total lift and drag on the airfoil can then be expressed as:

$$D = R'_x - F_{x_{cfj}} \tag{5}$$

$$L = R'_y - F_{y_{cfj}} \tag{6}$$

where R'_x and R'_y are the surface integral of pressure and shear stress in x (drag) and y (lift) direction excluding the internal ducts of injection and suction. For CFJ wing simulations, the total lift and drag are calculated by integrating Eqs.(5) and (6) in the spanwise direction.

2.2 Jet Momentum Coefficient

The jet momentum coefficient C_μ is a parameter used to quantify the jet intensity. It is defined as:

$$C_\mu = \frac{\dot{m} V_j}{\frac{1}{2}\rho_\infty {V_\infty}^2 S} \tag{7}$$

where $\dot{m}$ is the injection mass flow, V_j is the mass-averaged injection velocity, ρ_∞ and V_∞ denote the free stream density and velocity, and S is the planform area.

2.3 Micro-compressor Power Coefficient

CFJ is implemented by mounting a pumping system inside the wing that withdraws air from the suction slot and blows it into the injection slot. The power consumption is determined by the jet mass flow and total enthalpy change as the following:

$$P = \dot{m}(H_{t1} - H_{t2}) \tag{8}$$

where H_{t1} and H_{t2} are the mass-averaged total enthalpy in the injection cavity and suction cavity respectively, P is the Power required by the pump and $\dot{m}$ the jet mass flow rate. Introducing P_{t1} and P_{t2} the mass-averaged total pressure in the injection and suction cavity respectively, the compressor efficiency η, and the total pressure ratio of the pump $\Gamma = \frac{P_{t1}}{P_{t2}}$, the power consumption is expressed as:

$$P = \frac{\dot{m} C_p T_{t2}}{\eta}(\Gamma^{\frac{\gamma-1}{\gamma}} - 1) \tag{9}$$

where γ is the specific heat ratio equal to 1.4 for air. The power coefficient is expressed as:

$$P_c = \frac{P}{\frac{1}{2}\rho_\infty V_\infty^3 S} \tag{10}$$

If we assume the pumping efficiency in Eqn. 9 as 100%, it represents the power required to achieve the fluid mechanics effect. The actual power depends on the pumping efficiency as indicated by Eqn. 9. Pumping efficiency would vary for different actuators. The CoFlow Jet micro-compressor actuators can achieve very good efficiency of 80% and above [17, 27, 28, 29]. A lower power required coefficient is essential for an AFC to be efficient and effective. If an AFC has high power required to be effective, it would be difficult to benefit the system as a whole. CoFlow jet AFC demonstrates both high effectiveness and high efficiency [18]. The power required is also a parameter that can be accurately measured in laboratories and simulation for CFJ AFC due to it zero-net-mass-flux feature.

2.4 Aerodynamic Efficiency

The conventional wing aerodynamic efficiency is defined as:

$$\frac{C_L}{C_D} \tag{11}$$

For the CFJ wing, the ratio above still represents the pure aerodynamic relationship between lift coefficient and drag coefficient. However since CFJ active flow control consumes energy, the ratio above is modified to take into account the energy consumption of the micro-compressor. The formulation of the corrected aerodynamic efficiency for CFJ wings is:

$$(\frac{C_L}{C_D})_c = \frac{C_L}{C_D + P_c} \tag{12}$$

where P_c is the micro-compressor power coefficient defined in Eqn. 10 and C_L and C_D are the lift and drag coefficients of the CFJ wing. If the micro-compressor power coefficient is set to 0, this formulation returns to the aerodynamic efficiency of a conventional airfoil.

2.5 CFD Simulation Setup

The FASIP(Flow-Acoustics-Structure Interaction Package) CFD code is used to conduct the numerical simulation. The 2D Reynolds Averaged Navier-Stokes (RANS) equations with one-equation Spalart-Allmaras(SA) turbulence model is used. A 3rd order WENO scheme for the inviscid flux [30, 31, 32, 33, 34, 35] and a 2nd order central differencing for the viscous terms [30, 34] are employed to discretize the Navier-Stokes equations. The low diffusion E-CUSP scheme used as the approximate Riemann solver suggested by Zha et al [31] is utilized with the WENO scheme to evaluate the inviscid fluxes. Implicit time marching method using Gauss-Seidel line relaxation is used to achieve a fast convergence rate [36]. Parallel computing is implemented to save wall clock simulation time [37].

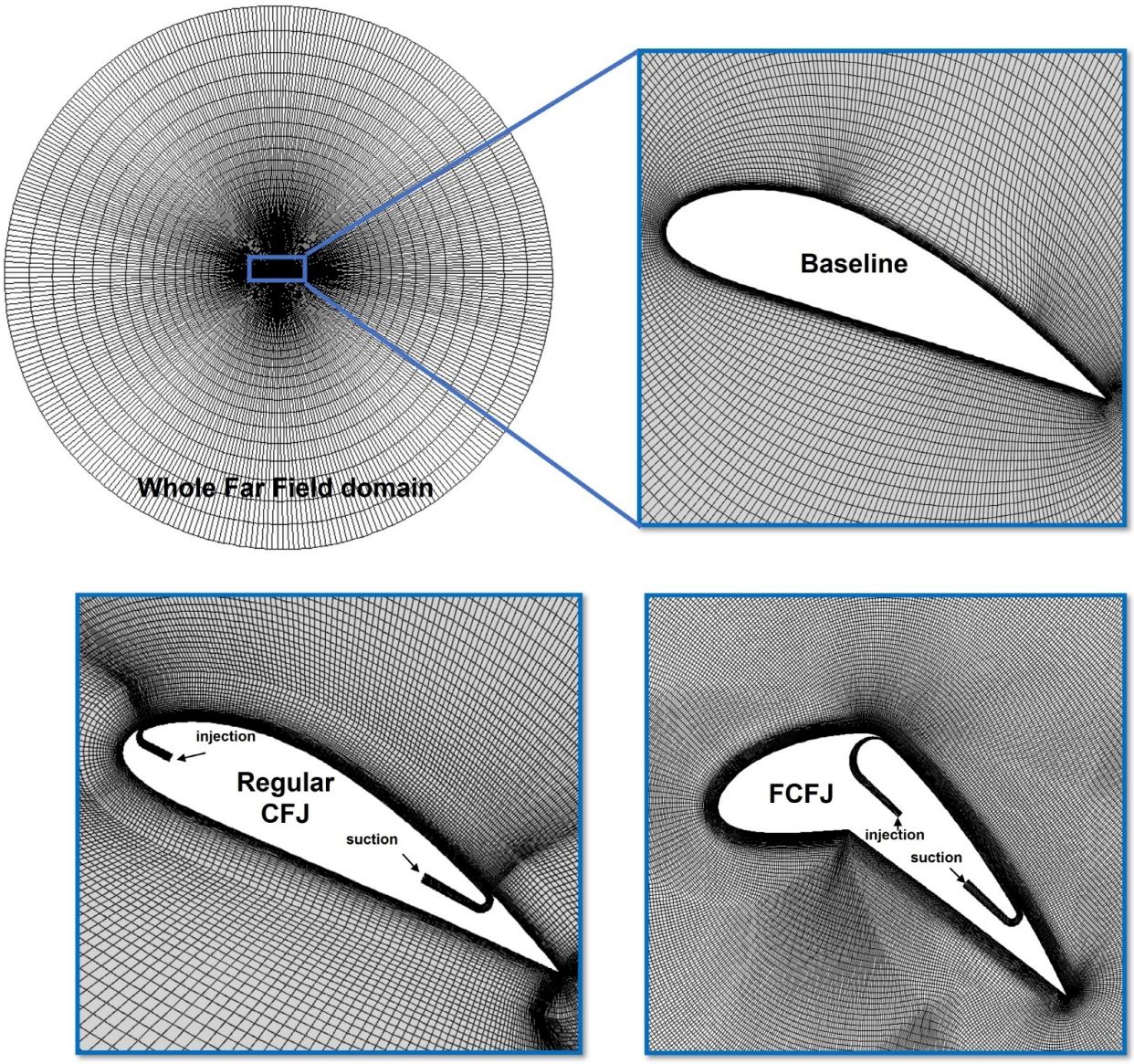

Figure 3: Computational mesh used in the current work.

2.6 Boundary Conditions

The 3rd order accuracy no slip condition is enforced on the solid surface with the wall treatment suggested in [38] to achieve the flux conservation on the wall. The far field boundary is located at 250 chord with a O-mesh topology. The computational mesh is shown in Fig. 3. Total pressure, total temperature and flow angles are specified at the upstream portion of the far field. Constant static pressure is applied at the downstream portion of the far field. The first grid point on the wing surface is placed at $y^+ \approx 1$.

3 Airfoil Geometry Parameters

Three airfoils are studied and compared in this study: 1) baseline NACA 6421 airfoil as shown in Fig. 3 (top), 2) an optimized regular CFJ NACA-6421 airfoil designed by Wang and Zha [21] shown in Fig. 3 (lower left), and 3) the flapped CFJ airfoil shown in Fig.3 (lower right). The FCFJ airfoil has the flap starting at 33%C. A parametric study has been conducted to understand the characteristics of FCFJ compared to regular CFJ and baseline. Table. 1 gives the detailed parameters of the airfoils based on NACA6421 baseline with the injection and suction slot size normalized by airfoil chord length (C). The rugular CFJ airfoil CFJ6421-SST150-SUC133-INJ065 is optimized by Lefebvre and Zha [18] for its high lift and cruise efficiency and is used as a reference to compare FCFJ. Flapped CFJ6421-SST150-SUC133 (FCFJ) airfoil is also developed based on the NACA 6421 airfoil which has the suction surface translation (SST) of 1.50%C and suction slot size of 1.33%C as the same as with the regular CFJ. In this study, flap deflection β is varied from 10° to 35°, and injection slot size is varied from 0.3%C to 1.2%C. The suction slot size is fixed at 1.33%C.

Table 1: Airfoil geometry parameters

Airfoil	Deflection Angle (β)	SST(%C)	INJ(%C)	SUC(%C)
NACA6421 Baseline	N/A	N/A	N/A	N/A
CFJ6421-SST150-SUC133-INJ065 (Regular CFJ)	N/A	1.5	0.65	1.33
Flapped CFJ6421-SST150-SUC133 (FCFJ)	10° - 35°	1.5	0.3 - 1.2	1.33

4 Simulated Cases

The Baseline and regular CFJ airfoils are simulated at various AoA as a comparison reference. The FCFJ airfoil is studied for its AoA and momentum coefficient effect listed in Table 2. The AoA of FCFJ is determined by the deflection angle β. In this study, we performed it for three Ma numbers, 0.17, 0.26 and 0.4, and the resulting Reynolds numbers are 5.43×10^4, 1.42×10^5 and 2.18×10^5 based on the chord length of 1m, respectively.

Table 2: Simulation cases used in the current work

Airfoil	Re	M_∞	AoA	C_μ
NACA6421 Baseline	5.43×10^4, 1.42×10^5, 2.18×10^5	0.17, 0.26, 0.4	0° - 20°	N/A
Regular CFJ	5.43×10^4, 1.42×10^5, 2.18×10^5	0.17, 0.26, 0.4	3° - 15°	0.03
FCFJ	5.43×10^4, 1.42×10^5, 2.18×10^5	0.17, 0.26, 0.4	6.4° - 23.5°	0.03 - 0.15

5 Results and Discussion

5.1 Baseline airfoil

The effect of angle of attack(AoA) on aerodynamic characteristics is investigated for the baseline NACA 6421 airfoil at Mach numbers(M) of 0.17, 0.26, and 0.4. Fig. 4 demonstrates that the C_L of the baseline NACA airfoil increases with increasing AoA. From 10° to 20°, C_L values at M0.26 and M0.4 are approximately 25% higher than those at M0.17 due to compressibility effect and higher Reynolds number. The slope of C_D with increasing AoA at M0.17 is significantly steeper than at higher Mach numbers. Consequently, as shown in Fig. 5, the aerodynamic efficiency, represented by C_L/C_D, is approximately 70% higher at both M0.26 and M0.4 than at M0.17. At M0.4, the maximum C_L/C_D is around 27, achieved at an AoA of 5° with a corresponding C_L of 0.88. The maximum C_L value is observed at M0.4, with only a 2% difference from M0.26. The trends in C_L/C_D for M0.26 and M0.4 are also very similar, with a difference of only 3%. However, for M0.17, the maximum C_L/C_D is approximately 16, with a corresponding C_L of 0.79, also achieved at an AoA of 5°. Compared with the results of the NACA 6421 experiment[39] at Reynolds number of 3.0×10^6, it is shown that for C_L, it decreases by about 33% at M0.17 and C_L/C_D by more than 65%.

Fig. 6 illustrates the flow field at an angle of attack of 10° for Mach numbers 0.17, 0.26, and 0.4, respectively. Flow separation is present in all the cases. Beyond this AoA, there is a rapid increase in drag coefficient (C_D), while the increase in lift coefficient (C_L) becomes insignificant as shown in Fig. 4.

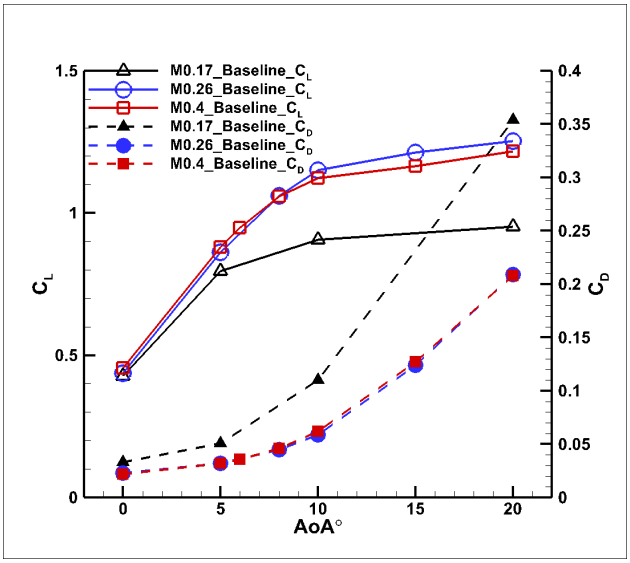

Figure 4: Lift and Drag coefficient for baseline

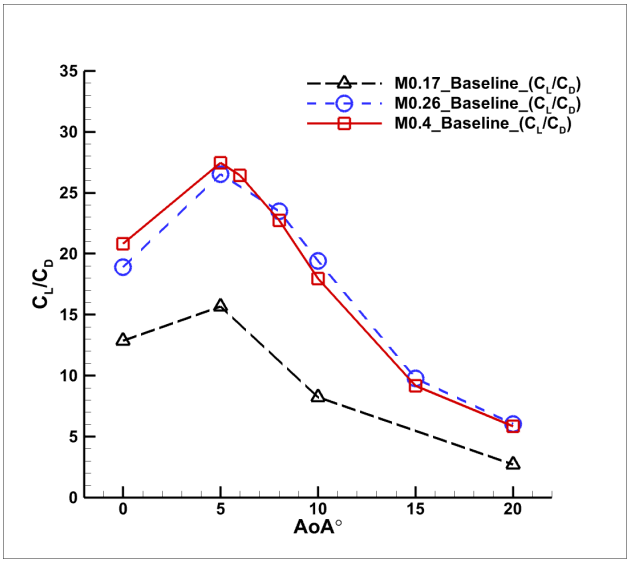

Figure 5: Aerodynamic efficiency for baseline

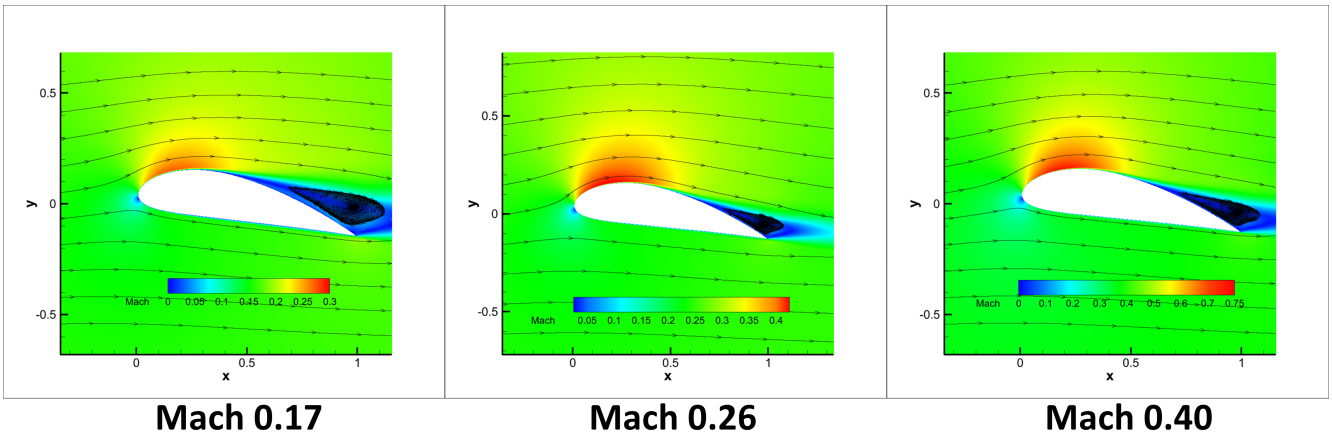

Figure 6: Baseline Flow field at AoA 10° according to Mach

5.2 Regular CFJ airfoil

The Regular CFJ airfoil exhibits a larger separation margin at C_μ of 0.03 compared to the Baseline airfoil. As shown in Fig. 7, the Regular CFJ airfoil achieves its maximum lift coefficient (C_L) at an angle of attack of 10° for all three Mach numbers(M) investigated: 0.17, 0.26, and 0.4 at C_μ of 0.03. Beyond this AoA, a significant increase in C_D and a decrease in C_L are observed. Please note that the CFJ airfoil can always remove the stall and increase the stall AoA by increasing C_μ. This study is to fix the C_μ at its optimal value of 0.03 for the cruise efficiency. Fig. 8 illustrates that the maximum cruising $(C_L/C_D)_c$ and the minimum P_c are also maximized at an AoA of 10°. Compared to the maximum C_L/C_D value of 5° for the Baseline airfoil, at M0.4, the Regular CFJ airfoil exhibits a 75% increase in C_L to 1.54 and a 55% increase in $(C_L/C_D)_c$ to 42.4. For M0.26, C_L increases by approximately 66% to reach 1.43, while the maximum $(C_L/C_D)_c$ increases by 42% to reach 37.8. At M0.17, C_L increases by about 60% to 1.28 and $(C_L/C_D)_c$ increases by 63% to 25.6. Fig. 9 presents the flow fields at AoA of 10° at M0.17, M0.26, and M0.4, respectively, demonstrating no flow separation for the Regular CFJ airfoil at C_μ of 0.03.

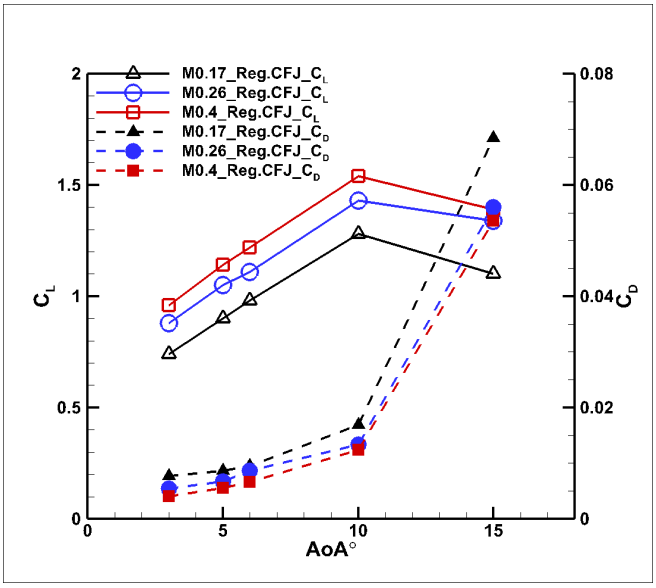

Figure 7: Lift and Drag coefficient for regular CFJ airfoil

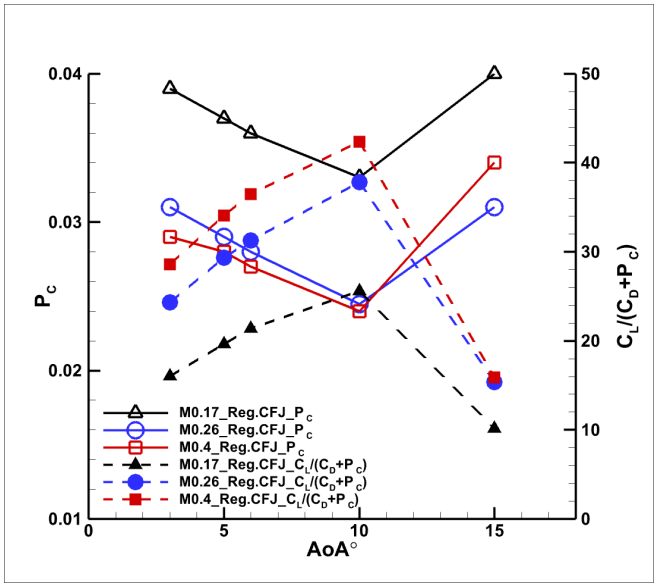

Figure 8: Power coefficient and Aerodynamic efficiency for regular CFJ airfoil

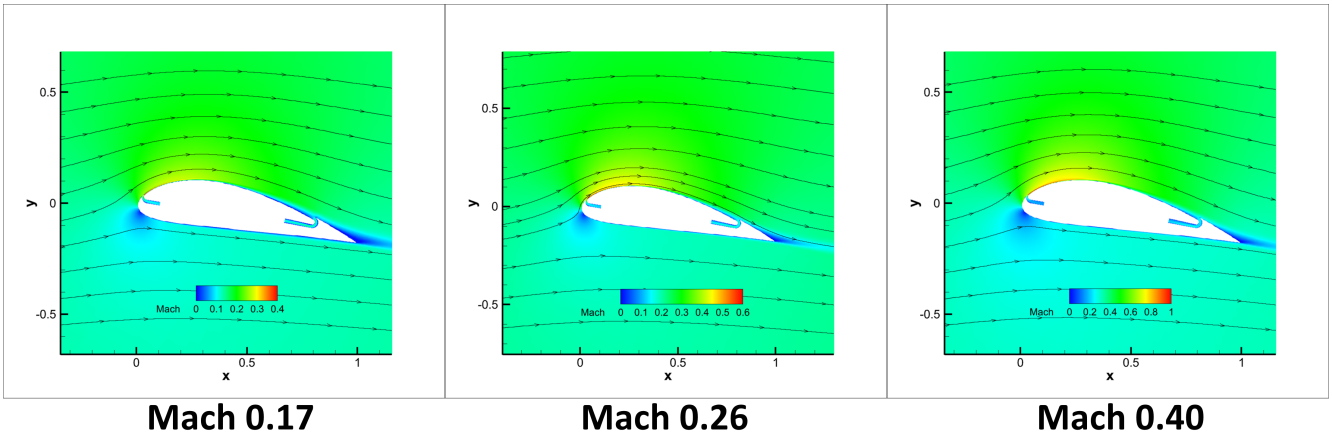

Figure 9: Flow field of Regular CFJ airfoil at AoA 10° according to Mach

5.3 Flapped CFJ airfoil

FCFJ is first performed with an injection size of 0.4%/C, which is the shape of the optimal results in [3]. Fig. 10 to Fig. 13 show C_L and $(C_L/C_D)_c$ against the C_μ from 0.03 to 0.07 with the flap deflection angle from β 10° to 35°. At β of 10°, C_L tends to increase as C_μ increases, but $(C_L/C_D)_c$ decreases. This is due to the increase in C_L/C_D but also the increase in Pc when C_μ increases as shown in Tables 3 - 5. The higher the Mach number, the greater the overall C_L and $(C_L/C_D)_c$ are obtained. For Mach of 0.4 case, $(C_L/C_D)_c$ is about 19.4 when the maximum CL is 1.72 for C_μ of 0.07 and β of 10°.

Fig. 11 is the result for β of 20°. The C_L tends to increase with increasing C_μ, but unlike β of 10°, the overall C_L is lowered at M=0.4. $(C_L/C_D)_c$ is also found to be the lowest at M=0.4. If β increases,

separation will occur at higher cruise Mach number as shown in Fig. 14, leading to an increase in drag and a decrease in lift. Looking at the flow field of M=0.4 at β of 20° in Fig. 14, a small flow separation is visible near the trailing edge. For β of 20° and C_μ of 0.07, the optimal Mach is 0.26 with the flow very well attached. The C_L has a value of 2 and higher, and $(C_L/C_D)_c$ can obtain a value around 30.

The results of β=30° are shown in Fig. 12. In the case of M=0.4, very large separation occurs in β=30° and β=35° at C_μ=0.1. As shown in Fig. 14. The C_L and $(C_L/C_D)_c$ are very low with the flow separation as expected. At $\beta = 30°$, the C_L of M=0.26 is slightly higher than that of M=0.17 with about 6% difference. For M=0.26 and β=30°, at C_μ 0.07 to 0.12, C_L is 3 to 4, which is more than 3 times higher than that of the baseline airfoil. $(C_L/C_D)_c$ has the highest value of 21.9 at C_μ=0.09 with C_L=3.6. C_L and $(C_L/C_D)_c$ at M=0.26 are better than the other Mach numbers, indicating that M=0.26 is the most efficient Mach number with a low P_c.

At β=35° as shown in Fig. 13, the trend of C_L is similar to that of β=30°. The case at Mach=0.26 also has the highest C_L and $(C_L/C_D)_c$ similar to at $\beta = 30°$. But $(C_L/C_D)_c$ is about 16, about 23% lower than β 30° due to increased drag with C_L=3.73. At M=0.17, C_L is about 6% lower at 3.53 and $(C_L/C_D)_c$ is about 26% lower at 12.6 The M=0.4 case has very poor results due to the massive flow separation.

Fig. 14 shows the Mach contours at different β angles and freestream Mach numbers. The flow reaches the peak Mach number on the suction surface slightly upstream of the injection slot at the deflection point of the flap. For the freestream Mach number of 0.17 at $\beta = 10°$ and 20°, the peak Mach number at the deflection point of the flap is about 0.3-0.4 with the jet Mach number of 0.65. At $\beta = 30°$ and 35°, the peak Mach number is about 0.5-0.7 with the jet Mach number about 0.9 just below the choked condition.

For the freestream Mach number of 0.26 at the flap deflection angle of $\beta = 10°,\ 20°,\ 30°$ and 35°, the peak Mach numbers in the flow fields are about 0.6, 0.8, 1.1, and 1.2 respectively. The jet Mach numbers are about 0.99, 1.06, 1.37, and 1.41 respectively. The flowfield is in the transonic regime with no shock wave with high lift coefficient benefited from the compressibility effect. At $\beta = 30°$, the injection slot is choked, but the Mach number of 1.37 is just at the limit before high entropy rise. It thus provides the optimal aerodynamic efficiency among the different cases of this study. When the β is increased to 35°, both the flow peak Mach number and the injection jet Mach number also increase. The overall aerodynamic efficiency is thus deteriorated.

For the freestream Mach number of 0.4 at the flap deflection angle of $\beta = 10°$ and 20°, the flow reaches the peak Mach number of 1.2 and 1.4 with the jet Mach number of 1.8 and 2.1. The jet is in the high loss range with shock waves as shown in the zoomed plots of Fig. 14. With the flap deflection angle further increase to 30° and above, the jet suffers excessive energy loss and the flow is very difficult to attach with higher supersonic Mach number and possible shock waves.

Table 3 to Table 5 list the results of M=0.17, M=0.26, and M=0.4. As mentioned earlier, the aerodynamic characteristics are the best at M=0.26. At C_μ of 0.1 and $\beta = 30°$, the C_L is 3.74 with the $(C_L/C_D)_c$ slightly over 20, which is only about 23% lower than C_L/C_D of the Baseline airfoil's peak efficient at AoA=5°, but the C_L is 335% higher.

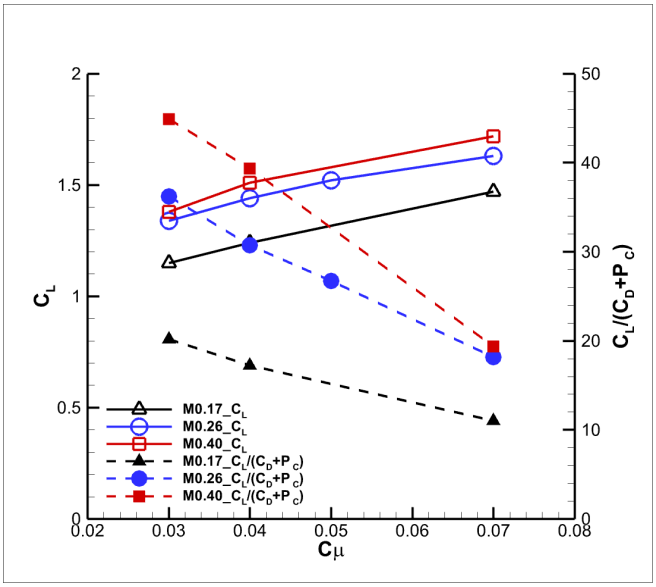

Figure 10: Lift coefficient and Aerodynamic efficiency for FCFJ airfoil at β=10°

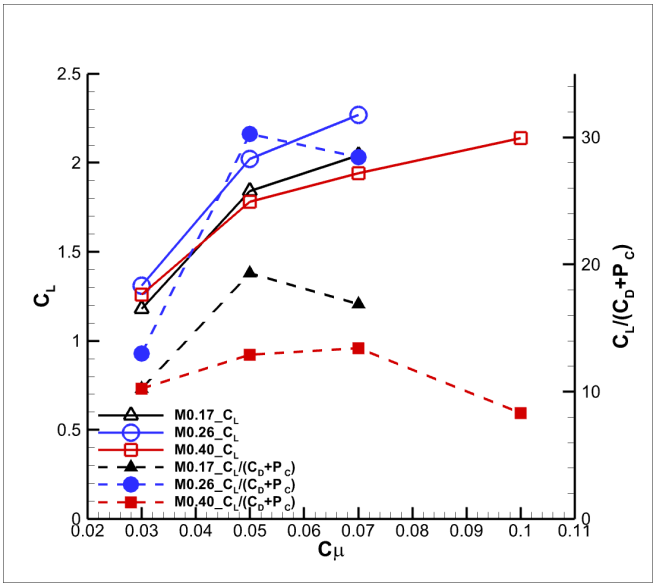

Figure 11: Lift coefficient and Aerodynamic efficiency for FCFJ airfoil at β=20°

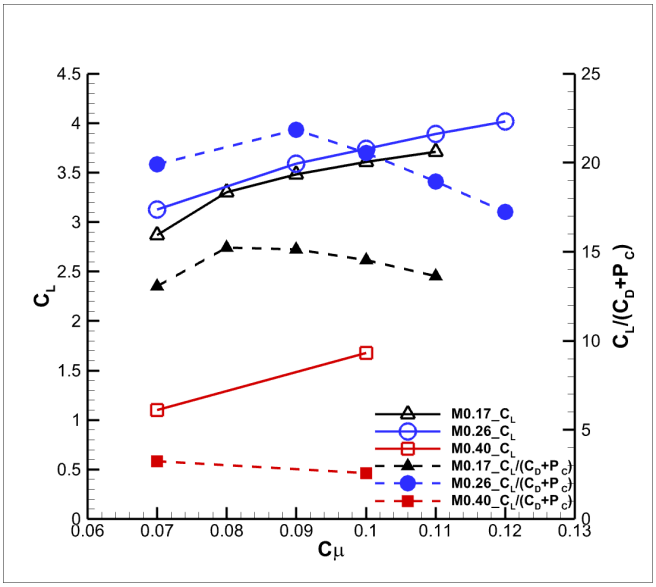

Figure 12: Lift coefficient and Aerodynamic efficiency for FCFJ airfoil at β=30°

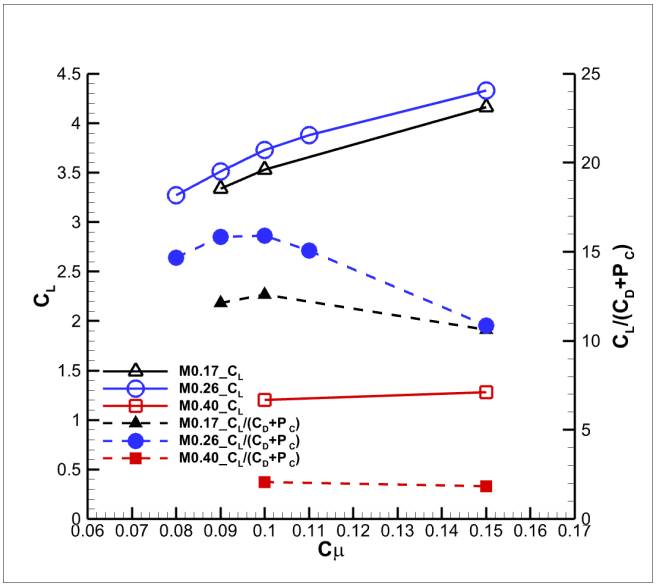

Figure 13: Lift coefficient and Aerodynamic efficiency for FCFJ airfoil at β=35°

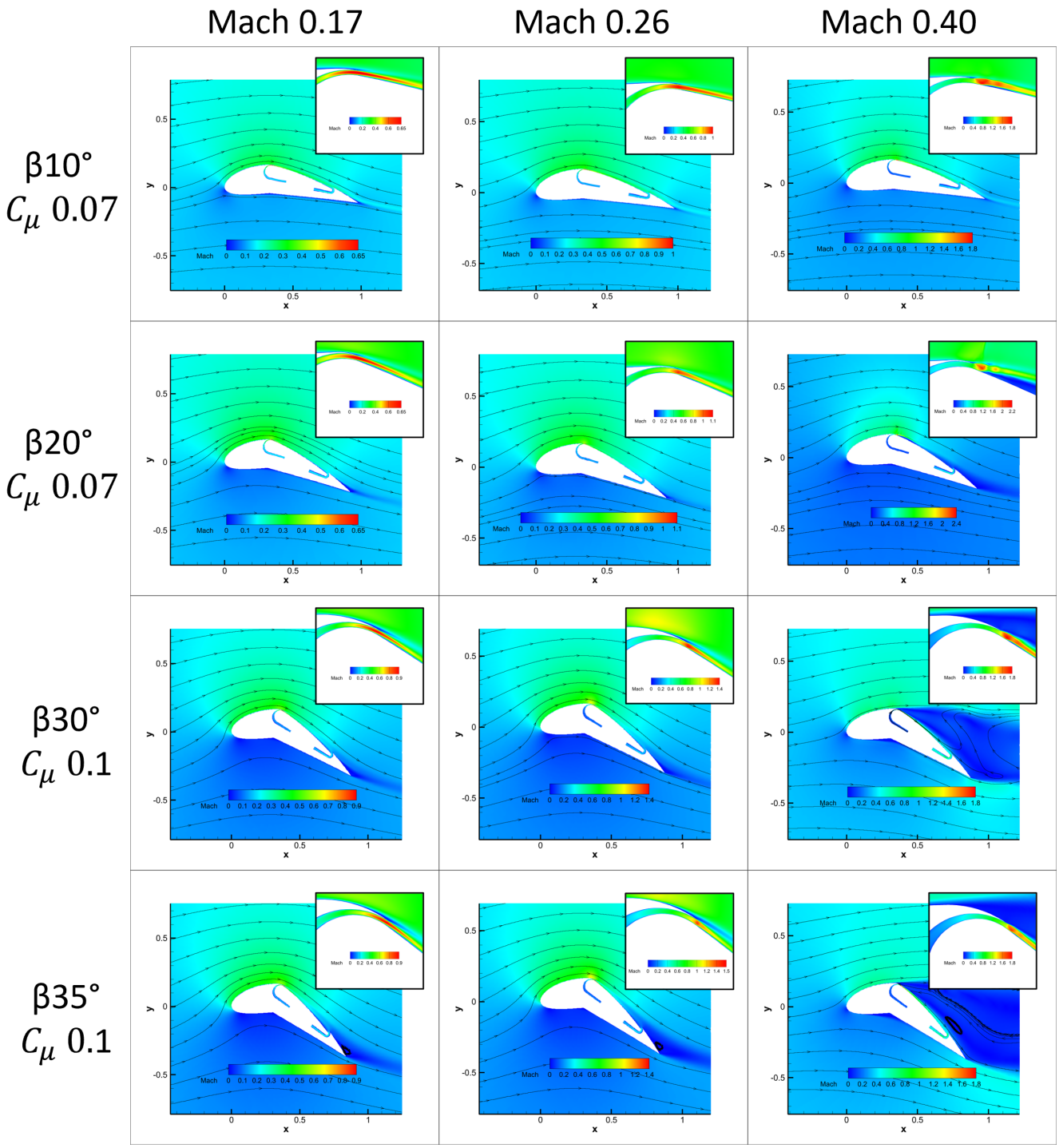

Figure 14: Flow field of Regular FCFJ airfoils

Table 3: Airfoil performance at different β for FCFJ airfoil at M0.17

β	AOA	C_μ	C_L	C_D	C_L/C_D	PR	Pc	Jet Mach	$(C_L/C_D)_c$
10	6.4	0.03	1.15	0.014	82.94	1.118	0.043	0.47	20.15
10	6.4	0.04	1.24	0.009	143.75	1.152	0.064	0.53	17.22
10	6.4	0.07	1.47	-0.006	-232.28	1.259	0.139	0.65	11.04
20	13.25	0.03	1.18	0.073	16.14	1.117	0.042	0.45	10.22
20	13.25	0.05	1.84	0.024	76.97	1.156	0.072	0.58	19.32
20	13.25	0.07	2.04	0.01	198.5	1.208	0.11	0.68	16.9
30	20	0.07	2.87	0.06	47.85	1.317	0.16	0.75	13.05
30	20	0.09	3.48	0.028	125.4	1.358	0.202	0.85	15.15
30	20	0.1	3.61	0.019	187.1	1.389	0.229	0.89	14.54
35	23.5	0.09	3.34	0.064	51.87	1.363	0.211	0.85	12.12
35	23.5	0.1	3.53	0.051	68.98	1.379	0.23	0.89	12.58
35	23.5	0.15	4.16	0.007	561.9	1.546	0.385	1.07	10.62

Table 4: Airfoil performance at different β for FCFJ airfoil at M0.26

β	AOA	C_μ	C_L	C_D	C_L/C_D	PR	Pc	Jet Mach	$(C_L/C_D)_c$
10	6.4	0.03	1.34	0.01	129.74	1.165	0.027	0.68	36.22
10	6.4	0.04	1.44	0.005	316.68	1.232	0.042	0.78	30.76
10	6.4	0.05	1.52	-0.002	-723.82	1.420	0.066	0.96	23.86
10	6.4	0.07	1.63	-0.008	-195.96	1.434	0.098	0.99	18.18
20	13.25	0.03	1.31	0.073	18.03	1.180	0.028	0.67	12.99
20	13.25	0.05	2.02	0.023	87.81	1.229	0.044	0.89	30.27
20	13.25	0.07	2.27	0.007	320.72	1.337	0.073	1.06	28.46
30	20	0.07	3.13	0.048	65.23	1.558	0.109	1.14	19.92
30	20	0.09	3.59	0.027	130.74	1.630	0.137	1.29	21.86
30	20	0.1	3.74	0.022	172.54	1.706	0.16	1.37	20.54
30	20	0.11	3.89	0.017	227.28	1.794	0.188	1.46	18.95
30	20	0.12	4.02	0.013	299.16	1.893	0.22	1.53	17.25
35	23.5	0.08	3.27	0.089	36.53	1.637	0.133	1.18	14.66
35	23.5	0.09	3.51	0.074	47.71	1.674	0.148	1.29	15.84
35	23.5	0.1	3.73	0.061	61.25	1.747	0.173	1.41	15.92
35	23.5	0.11	3.88	0.053	72.73	1.839	0.204	1.51	15.07
35	23.5	0.15	4.33	0.038	113.54	2.273	0.36	1.89	10.86

Table 5: Airfoil performance at different β for FCFJ airfoil at M0.4

β	AOA	C_μ	C_L	C_D	C_L/C_D	PR	Pc	Jet Mach	$(C_L/C_D)_c$
10	6.4	0.03	1.38	0.01	136.81	1.355	0.021	1.11	44.94
10	6.4	0.04	1.51	0.004	384.31	1.528	0.035	1.34	39.33
10	6.4	0.07	1.72	-0.007	-237.43	2.081	0.096	1.81	19.38
20	13.25	0.03	1.26	0.094	13.42	1.523	0.029	1.11	10.26
20	13.25	0.05	1.78	0.061	29.04	2.123	0.077	1.92	12.92
20	13.25	0.07	1.94	0.008	256.61	2.705	0.137	2.11	13.4
20	13.25	0.1	2.14	0.002	1043.11	3.840	0.255	2.42	8.33
30	20	0.07	1.1	0.205	5.35	2.729	0.133	1.49	3.24
30	20	0.1	1.68	0.447	3.76	3.279	0.209	1.81	2.56
35	23.5	0.1	1.2	0.359	3.33	3.281	0.216	1.72	2.08
35	23.5	0.15	1.28	0.351	3.65	4.210	0.352	2.05	1.82

6 Conclusion

This paper presents a numerical study of a 2D Flapped Coflow Jet (FCFJ) airfoil specifically designed for low Reynolds number conditions in the Martian atmosphere. The study investigates the aerodynamic performance of the FCFJ airfoil at freestream Mach numbers of 0.17, 0.26, and 0.4 and flap deflection angle of 10°, 20°, 30°, and 35°. When the Mach number is 0.26 and the deflection angle β is 30 degrees, the airfoil exhibits the most promising results in terms of lift coefficient(C_L) and corrected aerodynamic efficiency $(C_L/C_D)_c$.

At Mach number 0.26, the numerical simulations demonstrate that the FCFJ airfoil can achieve a lift coefficient of 3.74, a lift-to-drag ratio(C_L/C_D) of 172.54, and a corrected aerodynamic efficiency of 20.5. While these results indicate a decrease in aerodynamic efficiency of approximately 23% compared to the baseline airfoil, the lift coefficient is 4.35 times higher, which is expected to overcome the challenges posed by the low atmospheric density on Mars. At Mach number of 0.17, the overall aerodynamic performance is slightly lower than that of Mach number of 0.26 probably because the flow is mostly incompressible. At freestream Mach number of 0.26, the flow is in the transonic regime with full compressible flow. At flap deflection angle of 30°, the flow peak Mach number is about 1.1 and the injection Mach number is at supersonic Mach number of 1.37 with low entropy loss. It provides the optimal aerodynamic efficiency. At freestream Mach number of 0.4, the flow is supersonic at flap deflection angle of 20° with the peak Mach number of 1.4 and injection jet Mach number of 2.1, which forms the shock waves in the jet region and the flow suffers high energy loss. Further increasing the flap deflection angle will increase the flow supersonic Mach number and the injection jet Mach number, which increases the CFJ energy loss and make the flow difficult to attach.

This study provides compelling evidence that the FCFJ flapped airfoil can significantly enhance the lift coefficient of airfoils operating in low Reynolds number environments, such as the Martian atmosphere. Further studies for 3D flows need to be done as the next step.

7 Acknowledgment

The financial support from Teaching Assistantship of the University of Miami are acknowledged. The computation was conducted at the IDSC of University of Miami.

Disclosure: The University of Miami and Dr. Gecheng Zha may receive royalties for future commercialization of the intellectual property used in this study. The University of Miami is also equity owner in CoFlow Jet, LLC, licensee of the intellectual property used in this study.

References

[1] Koji FUJITA, Remi LUONG, Hiroki NAGAI, Keisuke ASAI, "Conceptual Design of Mars Airplane," *Trans. JSASS Aerospace Tech. Japan, Vol.10, No.ists28, pp.5-10*, 2012.

[2] Witold J.F.Koning, Ethan A.Romander, Wayne Johnson, "Optimization of Low Reynolds Number Airfoils for Martian Rotor Applications Using an Evolutionary Algorithm," *AIAA SciTech, AIAA-2020-0084, Orlando, Florida, USA*, 2020.

[3] Jaehyoung Jeon, Yan Ren, and Gecheng Zha, "Toward Ultra-High Cruise Lift Coefficient Using Flapped CoFlow Jet Airfoil," *AIAA SciTech Forum, AIAA 2023-1008, January 23-27, https://doi.org/10.2514/6.2023-1008*, 2023.

[4] Jaehyoung Jeon, Brendan McBreen, Yan Ren, and Gecheng Zha, "Study of 3D Flapped CoFlow Jet Wings for Ultra-High Cruise Lift Coefficient," *AIAA Aviation Forum, AIAA 2023-4436, June 12-16, https://doi.org/10.2514/6.2023-4436*, 2023.

[5] G.-C. Zha and D. C. Paxton, "A Novel Flow Control Method for Airfoil Performance Enhancement Using Co-Flow Jet." *Applications of Circulation Control Technologies*, Chapter 10, p. 293-314, Vol. 214, Progress in Astronautics and Aeronautics, AIAA Book Series, Editors: Joslin, R. D. and Jones, G.S., 2006.

[6] G.-C. Zha, W. Gao, and C. Paxton, "Jet Effects on Co-Flow Jet Airfoil Performance," *AIAA Journal, No. 6,*, vol. 45, pp. 1222–1231, 2007.

[7] G.-C. Zha, C. Paxton, A. Conley, A. Wells, and B. Carroll, "Effect of Injection Slot Size on High Performance Co-Flow Jet Airfoil," *AIAA Journal of Aircraft*, vol. 43, 2006.

[8] G.-C. Zha, B. Carroll, C. Paxton, A. Conley, and A. Wells, "High Performance Airfoil with Co-Flow Jet Flow Control," *AIAA Journal*, vol. Vol.45, No.8,, pp. 2087–2090, 2008.

[9] Wang, B.-Y. and Haddoukessouni, B. and Levy, J. and Zha, G.-C., "Numerical Investigations of Injection Slot Size Effect on the Performance of Co-Flow Jet Airfoil," *Journal of Aircraft*, vol. Vol. 45, No. 6,, pp. pp.2084–2091, 2008.

[10] B. P. E. Dano, D. Kirk, and G.-C. Zha, "Experimental Investigation of Jet Mixing Mechanism of Co- Flow Jet Airfoil." AIAA-2010-4421, 5th AIAA Flow Control Conference, Chicago, IL, 28 Jun - 1 Jul 2010.

[11] B. P. E. Dano, G.-C. Zha, and M. Castillo, "Experimental Study of Co-Flow Jet Airfoil Performance Enhancement Using Micro Discreet Jets." AIAA Paper 2011-0941, 49th AIAA Aerospace Sciences Meeting, Orlando, FL, 4-7 January 2011.

[12] A. Lefebvre, B. Dano, W. Bartow, M. Fronzo, and G. Zha, "Performance and energy expenditure of coflow jet airfoil with variation of mach number," *Journal of Aircraft*, vol. 53, no. 6, pp. 1757–1767, 2016.

[13] A. Lefebvre, G-C. Zha, "Numerical Simulation of Pitching Airfoil Performance Enhancement Using Co-Flow Jet Flow Control," *AIAA paper 2013-2517*, June 2013.

[14] A. Lefebvre, G-C. Zha, "Cow-Flow Jet Airfoil Trade Study Part I : Energy Consumption and Aerodynamic Performance," *AVIATION, 32nd AIAA Applied Aerodynamics Conference, AIAA-2014-2682*, June 2014.

[15] A. Lefebvre, G-C. Zha, "Cow-Flow Jet Airfoil Trade Study Part II : Moment and Drag," *AVIATION, 32nd AIAA Applied Aerodynamics Conference, AIAA-2014-2683*, June 2014.

[16] Yunchao Yang, Gecheng Zha, "Super-Lift Coefficient of Active Flow Control Airfoil: What is the Limit?," *AIAA Paper 2017-1693, AIAA SCITECH2017, 55th AIAA Aerospace Science Meeting, Grapevine, Texas, 9-13 January 2017*, 2017.

[17] Gecheng Zha, Yunchao Yang, Yan Ren, Brendan McBreen, "Super-Lift and Thrusting Airfoil of Coflow Jet Actuated by Micro-Compressors," *AIAA Paper-2018-3061, AIAA AVIATION Forum 2018, Flow Control Conference, June 25-29*, 2018.

[18] Lefebvre, A. and Zha, G.-C., "Trade Study of 3D Co-Flow Jet Wing for Cruise Performance." AIAA Paper 2016-0570, AIAA SCITECH2016, AIAA Aerospace Science Meeting, San Diego, CA, 4-8 January 2016.

[19] Kewei Xu, Gecheng Zha, "High Control Authority 3D Aircraft Control Surfaces Using Co-Flow Jet," *AIAA Aviation 2019 Forum, AIAA-2019-3168, 17-21 June, https://doi.org/10.2514/6.2019-3168*, 2019.

[20] Kewei Xu, Yan Ren, Gecheng Zha, "Numerical Analysis of Energy Expenditure for Co-Flow Wall Jet Separation Control," *AIAA Journal, published online: 11 Jan 2022, doi.org/10.2514/1.J061015*, 2022.

[21] Yang Wang and Gecheng Zha, "Study of Mach Number Effect for 2D Co-Flow Jet Airfoil at Cruise Conditions," *AIAA Paper 2019-3169, AIAA Aviation 2019 Forum, 17-21 June 2019, Dallas, Texas*, 2019.

[22] Yang Wang and Gecheng Zha, "Study of Mach Number Effect for 3D Co-Flow Jet Wings at Cruise Conditions," *AIAA Paper 2020-0045, AIAA SciTech Forum, 6-10 January 2020, Orlando, FL*, 2020.

[23] Yan Ren, Gecheng Zha, "Performance Enhancement by Tandem Wings Interaction of CoFlow Jet Aircraft," *AIAA Paper 2021-1823, AIAA SciTech Forum, 11–15; 19–21 January 2021, VIRTUAL EVENT*, 2021.

[24] Yang Wang, Yunchao Yang and Gecheng Zha, "Study of Super-Lift Coefficient of Co-Flow Jet Airfoil and Its Power Consumption," *AIAA Paper 2019-3652, AIAA Aviation 2019 Forum, 17-21 June 2019, Dallas, Texas* , 2019.

[25] Zha, G.-C,, "Feasibility Study of Deflected Slipstream Airfoil for VTOL Hover Enabled by CoFlow Jet," *AIAA Aviation Forum 2023-4279, 12–16 June 2023, San Diego, CA*, 2023.

[26] Kewei Xu, Yan Ren, and Gecheng Zha, "Separation Control by Co-Flow Wall Jet," *AIAA Paper 2021-2946, AIAA AVIATION Forum, August 2-6*, 2021.

[27] Kewei Xu and Gecheng Zha, "DESIGN OF HIGH SPECIFIC SPEED MIXED FLOW MICRO-COMPRESSOR FOR CO-FLOW JET ACTUATORS," *ASME Paper GT-2019-90980, ASME Turbo Expo*, 2019.

[28] Paula A. Barrios, Yan Ren, GeCheng Zha, "Simulation of 3D Co-Flow Jet Airfoil Control with Micro-Compressor Actuator at High Angles of Attack," *AIAA AVIATION 2023 Forum, 12-16 June 2023, San Diego, CA*, 2023.

[29] Paula A. Barrios, Yan Ren, GeCheng Zha, "Simulation of 3D Co-Flow Jet Airfoil with Integrated Micro-Compressor Actuator at Different Cruise Mach Numbers," *AIAA Paper-2023-2118, AIAA SCITECH 2023*, 2023.

[30] Y.-Q. Shen and G.-C. Zha, "Large Eddy Simulation Using a New Set of Sixth Order Schemes for Compressible Viscous Terms ," *Journal of Computational Physics*, vol. 229, pp. 8296–8312, 2010.

[31] Zha, G.C., Shen, Y.Q. and Wang, B.Y., "An improved low diffusion E-CUSP upwind scheme ," *Journal of Computer and Fluids*, vol. 48, pp. 214–220, Sep. 2011.

[32] Y.-Q. Shen and G.-Z. Zha , "Generalized finite compact difference scheme for shock/complex flowfield interaction," *Journal of Computational Physics*, vol. doi:10.1016/j.jcp.2011.01.039, 2011.

[33] Shen, Y.-Q. and Zha, G.-C. and Wang, B.-Y., " Improvement of Stability and Accuracy of Implicit WENO Scheme," *AIAA Journal*, vol. 47, No. 2, pp. 331–344, 2009.

[34] Shen, Y.-Q. and Zha, G.-C. and Chen, X.-Y., " High Order Conservative Differencing for Viscous Terms and the Application to Vortex-Induced Vibration Flows," *Journal of Computational Physics*, vol. 228(2), pp. 8283–8300, 2009.

[35] Shen, Y.-Q. and Zha, G.-C. , " Improvement of the WENO Scheme Smoothness Estimator," *International Journal for Numerical Methods in Fluids*, vol. DOI:10.1002/fld.2186, 2009.

[36] G.-C. Zha and E. Bilgen, "Numerical Study of Three-Dimensional Transonic Flows Using Unfactored Upwind-Relaxation Sweeping Algorithm," *Journal of Computational Physics*, vol. 125, pp. 425–433, 1996.

[37] B.-Y. Wang and G.-C. Zha, "A General Sub-Domain Boundary Mapping Procedure For Structured Grid CFD Parallel Computation," *AIAA Journal of Aerospace Computing, Information, and Communication*, vol. 5, No.11, pp. 2084–2091, 2008.

[38] Y.-Q. Shen, G.-C. Zha, and B.-Y. Wang, "Improvement of Stability and Accuracy of Implicit WENO Scheme ," *AIAA Journal*, vol. 47, pp. 331–344, 2009.

[39] EASTMAN N.JACOBS, KENNETH E. WARD, and ROBERT M.PINKERTON, "THE CHARACTERISTICS OF 78 RELATED AIRFOIL SECTIONS FROM TESTS IN THE VARIABLE-DENSITY WIND TUNNEL," *REPORT No.460*, 1935.